

Power-SLIC: Fast Superpixel Segmentations by Diagrams

Maximilian Fiedler

Zentrum Mathematik, Technische Universität München
D-85748 Garching bei München, Germany

maximilian.fiedler@tum.de

Andreas Alpers

University of Liverpool, Department of Mathematical Sciences
Liverpool L69 7ZL, UK

andreas.alpers@liverpool.ac.uk

Abstract

Superpixel algorithms grouping pixels with similar color and other low-level properties are increasingly used for pre-processing in image segmentation. In recent years, a focus has been placed on developing geometric superpixel methods that facilitate the extraction and analysis of geometric image features. Diagram-based superpixel methods are important among the geometric methods as they generate compact and sparsely representable superpixels. Introducing generalized balanced power diagrams to the field of superpixels, we propose a diagram method called Power-SLIC. Power-SLIC is the first geometric superpixel method to generate piecewise quadratic boundaries. Its speed, competitive with fast state-of-the-art methods, is unprecedented for diagram approaches. Extensive computational experiments show that Power-SLIC outperforms existing diagram approaches in boundary recall, under segmentation error, achievable segmentation accuracy, and compression quality. Moreover Power-SLIC is robust to Gaussian noise.

1. Introduction

Superpixels are small, non-overlapping groups of connected, perceptually homogeneous pixels. Since its introduction by Ren and Malik in 2003 [32], superpixel generation has become an important pre-processing step in many imaging applications such as object localization [19], multi-class segmentation [20], optical flow [30], body model estimation [31], object tracking [41], depth estimation [42], and image denoising [28].

Superpixels reduce the number of inputs for subsequent algorithms and provide meaningful image representations from which application-relevant parameters can be

extracted. It is commonly desirable that superpixels adhere well to object boundaries, are quickly generated, and compact [2, 5, 35].

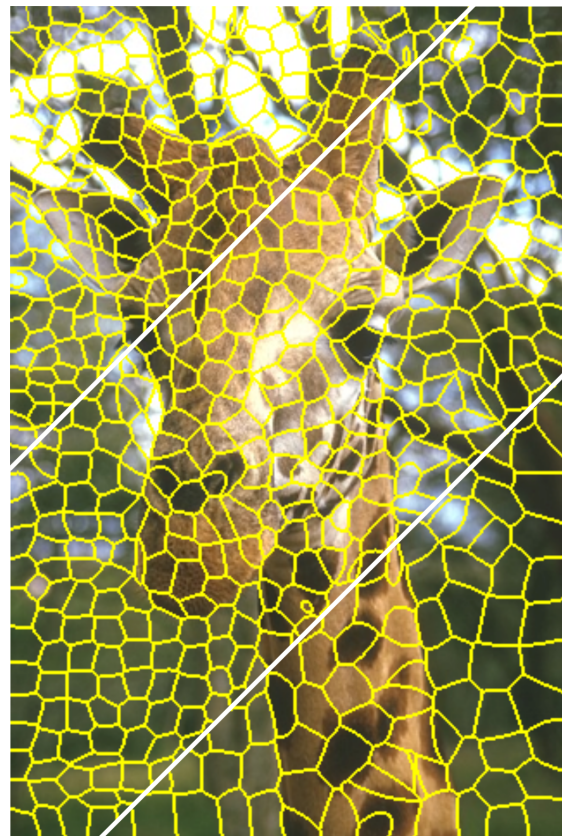


Figure 1. Superpixel segmentation using Power-SLIC with 900, 600, and 300 superpixels.

Traditionally, superpixel algorithms are pixel-based because they operate on the pixel level, generating regions delimited by sets of pixels. Such pixel-level superpixel rep-

representations can often approximate small details and adhere well to boundaries. However, they are generally non-compact and free of higher-level geometric information.

Addressing this aspect, recent studies [3, 6, 15, 22, 27], have focused on developing geometric superpixel methods. These methods partition the image into small, preferably size-controllable, geometric objects, e.g., polygonal cells. As these objects ‘live’ in the continuous world, they provide a resolution-independent superpixel representation and facilitate geometric manipulations, feature extractions, and other higher-level geometric post-processing tasks. The applicative potential of geometric superpixel methods has been demonstrated for diverse computer vision tasks such as object contouring [6, 27], image vectorization [12], image compression [17, 27], and segmentations of scenes containing man-made environments or other strong geometric signatures [15].

Many pixel methods, e.g., [2, 25, 26, 39], employ Voronoi diagrams as intermediate structure, but they depart from it to better control the sizes and shapes of the superpixels. In contrast, the geometric methods Varane [14, 15] and, most recently, ECCPD [27] return diagram cells as superpixels that are compact and sparsely representable. However, both of these diagram approaches employ time-consuming post-optimization to control the superpixel sizes and shapes. Motivated by unifying and extending the diagram approaches, we propose a novel method, called Power-SLIC, which handles non-linear boundaries and brings the speed of state-of-the-art pixel methods to the geometric world.

1.1. Technical Contribution

The main technical contribution of our work is that we bridge the gap between pixel and geometric superpixel methods by utilizing the following three techniques: (i) a deep connection between constrained clustering and diagrams from [8] (see Theorem 1) to control the diagram cell sizes, (ii) the heuristic [36] based on this, and (iii) SLIC’s initialization & assignment step.

Contribution to the geometric world: A diagram method that, for the first time, has a speed similar to fast pixel-based methods and that outperforms existing approaches in boundary recall, under segmentation error, achievable segmentation accuracy, and compression quality. To our knowledge, this is the first geometric approach capable of generating non-linear superpixel boundaries.

Contribution to the pixel world: A fast and noise-robust method that clusters pixels into superpixels but provides the benefits of diagram approaches such as providing sparse geometric superpixel representations by diagrams, facilitating geometric image operations, and providing relatively compact and regular superpixels at the same time.

1.2. Related Works

We briefly review superpixel algorithms classified into two groups: pixel methods and geometric methods. For a comprehensive evaluation see [35, 40].

Pixel methods Many popular state-of-the-art superpixel generation methods are pixel-based. A large number of pixel methods, such as SLIC [2], VCells [39], TurboPixel [23], and SEEDS [38], employ clustering algorithms refining the clusterings until a convergence criterion is satisfied. SLIC, and variants such as SLIC0 [1], SNIC [3], Manifold-SLIC [25], and Intrinsic Manifold-SLIC [26], are particularly popular due to their simplicity and high performance.

Other algorithms, such as ERS [24] and Normalized Cuts [32], formulate the superpixel generation task as an optimization problem on a graph structure.

It has been noted several times (e.g., in [7, 33, 35]) that the performance of superpixel algorithms degrades severely as noise levels increase. To address this issue, [13] proposes a Mahalanobis-based k -means variant (NR-SLIC). The Mahalanobis distance is also used in [5] and [11], which introduce a Gaussian mixture model (GMMSP) and a unimodular Gaussian generative model, respectively. Gaussian mixture models based on Bayesian or Normal-Inverse Wishart priors for the covariances are given in [18, 37]. Common to these approaches is that they consider Mahalanobis distances for both the pixels’ spatial and color components. Their clusterings in 5D can be viewed as resulting from five-dimensional generalized balanced power diagrams (GBPDs) [4]. As projections from 5D into 2D, their spatial cell boundaries are, however, rather irregular; see GMMSP and NR-SLIC in Fig. 5. Our approach utilizes the Mahalanobis distance only for the spatial components of the pixels, resulting, as we will demonstrate, in two-dimensional GBPDs with smooth, quadratic cell boundaries.

Geometric methods Geometric methods (also known as resolution-independent or polygonal decomposition methods) aim at extracting continuous parameter representations of the superpixel boundaries.

The algorithm from [15], referred to as Varane [14], partitions the image into convex polygonal superpixels by building Voronoi diagrams that conform to preliminarily detected line segments. The color values inside these Voronoi cells can be approximated; for example, [12] proposes an approximation by polynomials. More general than Voronoi diagram cells, ECCPD from [27] proposes to segment images into power diagram cells. The algorithm iterates between updates of sites and weights and applies an edge-alignment optimization step.

Meshes of convex polygonal cells that are guaranteed to have no small angles are generated in [17]. An improved method is given in [22]. The algorithms SNIC and SNICPOLY from [3] produce superpixels with piecewise linear boundaries. KIPPI from [6] uses a kinetic approach that extends line segments until they meet each other. KIPPI can generate polygons of different sizes, avoiding oversegmentations of large uniform areas, but it does not allow explicit control over the number of superpixels. A Delaunay Point Process (DPP), which segments images into triangular patches, is proposed in [16].

Noticeably, many algorithms compute an intermediate diagram structure. Diagrams are returned as final superpixel segmentation only in Varane and ECCPD. Therefore, we refer to them as diagram approaches. They return Voronoi and power diagrams, respectively, which have linear boundaries. In contrast, our diagram class of GBPDs contains the latter diagram classes as subclasses. Boundaries can be quadratic, but the cell convexity may be lost.

2. Overview of our Approach

We borrow the initialization & assignment step from SLIC (Simple Linear Iterative Clustering) [2] to obtain possibly non-connected groups of pixels, which typically have a high boundary adherence but fuzzy boundaries. In contrast to SLIC’s post-processing, which guarantees connected superpixels, we compute a generalized balanced power diagram (GBPD) based on the spatial Mahalanobis distance determined for every previously obtained group of pixels. The cells of the GBPD will ultimately be the resulting superpixels. As the computation of GBPDs can be time-consuming, we approximate it to achieve a competitive running time. A high-level visualization of Power-SLIC is illustrated in Fig. 2.

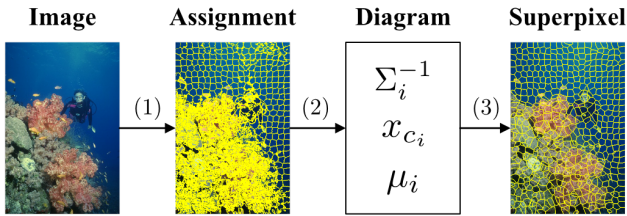


Figure 2. Main steps of Power-SLIC: (1) Perform SLIC’s initialization & assignment step. (2) Extract diagram parameters from the assignment yielding a geometric representation of the superpixels. (3) Assign each pixel to its containing diagram cell (yielding a pixel representation of the superpixels).

SLIC’s assignment phase ideally suits our purposes, as it constructs a five-dimensional Voronoi diagram, a special case of a GBPD, with linear boundaries. Our approach aims at approximating and regularizing this 5D structure by a GBPD with quadratic cell boundaries in the two spatial dimensions.

3. SLIC’s Initialization & Assignment Phase

SLIC [2] is seen as one of the most popular and widely used methods for superpixel generation. Given a color image of N pixels, SLIC clusters the pixels within the five-dimensional space (x_p, l_p) , with x_p denoting the spatial position of pixel p (a two-dimensional vector) and l_p its color (a three-dimensional vector) in the CIELAB color space. The algorithm is divided into an initialization & assignment and a post-processing phase. The latter phase ensures connectivity by reassigning near-by superpixels. As we do not make use of this phase, we omit a description.

Initialization & Assignment SLIC takes as its input two arguments k and m , with k specifying the targeted number of superpixels and m denoting a compactness parameter. Throughout this paper, we use $m = 10$ as this is SLIC’s default value. Initially, SLIC samples cluster centers with spatial positions from a square grid spaced $h = \sqrt{N/k}$ pixels apart. Subsequently, pixels are assigned to their closest cluster center. However only local assignments of pixels lying within a $2h \times 2h$ spatial window around a cluster center are considered to improve performance. Proximity is measured by a weighted Euclidean distance. The second parameter, m , determines the weight of the Euclidean distance in the color space. For a pixel p and a center c , the squared distance d^2 is given by:

$$d^2(p, c) = \|x_p - x_c\|_2^2 + \frac{h^2}{m^2} \cdot \|l_p - l_c\|_2^2. \quad (1)$$

As in traditional k -means, the centers are updated as the centroids of the updated clusters, and the process is iterated until some stopping criterion is fulfilled.

4. Generalized Balanced Power Diagrams

Generalized balanced power diagrams (GBPDs) [4] generalize the concept of power diagrams, which themselves generalize the famous Voronoi diagrams. Here, we are given a set of k distinct sites $S = \{s_1, \dots, s_k\} \subseteq \mathbb{R}^d$. Each site is equipped with a local ellipsoidal norm defined by a positive definite symmetric matrix $A_i \in \mathbb{R}^{d \times d}$. The norm $\|\cdot\|_{A_i}$ is defined as $\|x\|_{A_i} := \sqrt{x^\top A_i x}$ for $x \in \mathbb{R}^d$, $i \in [k]$. Moreover, let μ_1, \dots, μ_k be scalars serving as additional balancing parameters.

For every $i \in [k]$, the generalized balanced power diagram cell is defined as:

$$P_i := \{x \in \mathbb{R}^d : \|x - s_i\|_{A_i}^2 + \mu_i \leq \|x - s_l\|_{A_l}^2 + \mu_l, \forall l \in [k]\}. \quad (2)$$

We call the k -tuple of cells (P_1, \dots, P_k) a generalized balanced power diagram (GBPD). Throughout this paper, we

consider only two-dimensional GBPDs, although our approach canonically extends to images and GBPDs in arbitrary dimensions.

Further, we remark that we obtain power diagrams in the special case in which each A_1, \dots, A_k are the identity matrix. If additionally $\mu_1 = \dots = \mu_k$, we obtain Voronoi diagrams.

5. Optimal Power-SLIC and Power-SLIC

Given the assignment L computed by SLIC's initialization & assignment phase, we propose computing the following statistics for each label i in L : the spatial center x_{c_i} , the spatial covariance matrix $\Sigma_i \in \mathbb{R}^{2 \times 2}$, and the area κ_i of each possibly non-connected component $C_i = \{x_p : L(p) = i\}$. From this we compute a GBPD with sites $s_i = x_{c_i}$ and matrices $A_i = \Sigma_i^{-1}$, such that the area of its cells P_i equals or approximates κ_i , $i \in [k]$. The cells P_1, \dots, P_k of the GBPD will be the resulting superpixels.

Optimal Power-SLIC We first present an algorithm to compute GBPDs as described above. As in [4], we can achieve this by exploiting a strong relation between constrained clustering and (anisotropic) power diagrams shown in [8] (see also [9]). We consider the following linear program:

$$\begin{aligned}
 \min \quad & \sum_{i=1}^k \sum_{j=1}^N \xi_{ij} \|x_{p_j} - s_i\|_{A_i}^2 \\
 \text{s.t.} \quad & \sum_{i=1}^k \xi_{ij} = 1, \quad j \in [N], \\
 & \sum_{j=1}^n \xi_{ij} = \kappa_i, \quad i \in [k], \\
 & \xi_{ij} \geq 0, \quad i \in [k], j \in [N].
 \end{aligned} \tag{P}$$

Its dual is given by:

$$\begin{aligned}
 \max \quad & \sum_{j=1}^N \eta_j - \sum_{i=1}^k \kappa_i \mu_i \\
 \text{s.t.} \quad & \eta_j \leq \|x_{p_j} - s_i\|_{A_i}^2 + \mu_i, \quad i \in [k], j \in [N].
 \end{aligned} \tag{D}$$

The problem modeled by (P) is the balanced least-squares assignment problem. The task is to assign x_{p_j} to sites in such a way that precisely κ_i of them are assigned to site s_i , for each $i \in [k]$, while the sum of squared distances of the assigned x_{p_j} to their assigned sites, measured via the norm $\|\cdot\|_{A_i}$, is minimized. As the constraint matrix of the problem is totally unimodular, there will be a binary optimal solution to (P), i.e., in this solution, ξ_{ij}^* is either 0 or 1 where $\xi_{ij}^* = 1$ if, and only if, x_{p_j} is assigned to site s_i .

Optimal solutions to (P) can be characterized in terms of GBPDs. To state this precisely, we apply the following notion: a diagram is said to induce a binary assignment if, and only if, all x_{p_j} assigned to the same cluster lie in the same diagram cell.

Theorem 1 (Special case of [10]) *A balanced assignment is a basic solution of the linear program (P) if and only if there exists a parameter vector $\mu \in \mathbb{R}^k$ such that the GBPD with parameters (A_i, s_i, μ_i) , $i \in [k]$, induces this binary assignment. Moreover, with a solution (μ^*, η^*) of Eq. (D) that fulfills strict complementary slackness, we can choose $\mu = \mu^*$.*

Hence, when optimally assigning pixels to superpixel centers, i.e., for $s_i = x_{c_i}$, superpixel areas prescribed to equal κ_i , and distance matrices $A_i = \Sigma_i^{-1}$, the resulting superpixels can be characterized by cells of a GBPD. Moreover, the diagram parameters are extracted from the dual solution and yield a low-dimensional, resolution-independent representation of the superpixels (an algebraic representation of the boundary between two neighboring cells is provided by the quadratic equation that results from changing the respective inequality relation in Eq. (2) to an equality relation).

In terms of computational complexity, we remark that (P) has Nk variables and $2N + k$ constraints. The linear program can, however, be solved in $\mathcal{O}(N^3)$ using the Hungarian method, for example. In our evaluation, we use the dual simplex of Gurobi [21]. To improve performance, we apply a locality assumption similar to SLIC by adding only those variables ξ_{ij} for which p_j lies within a regional window of the center c_i . To ensure that every pixel is assigned, we choose this window to be the smallest bounding box of C_i . The resulting algorithm, called Optimal Power-SLIC, is summarized in Algorithm 3.

We found that building the model takes up most of the time, while solving the model usually requires less than 10 s per image. This suggests that more significant speed-ups can be achieved by avoiding Gurobi calls, e.g., by using a more specialized and adapted solver, such as min-cost flow.

Power-SLIC To match the SLIC linear running time, we now introduce a heuristic version of Optimal Power-SLIC, which we call Power-SLIC. The main ideas are rooted in two key observations.

First, we observe that most of the computation time in Optimal Power-SLIC is spent on computing μ_1, \dots, μ_k while the sites and norm matrices of the diagram are essentially readily available. To effect a significant speed-up, we replace the computation of the optimal μ_i with an estimation. The idea is to think of μ_i as a scaling factor and estimate it such that the ellipsoid given by the inverse covariance matrix $A_i = \Sigma^{-1}$ has an area equal to κ_i . Thus, we

Data: Image, targeted number k of superpixels.
Result: Assignment, GBPD.
Run SLIC’s initialization & assignment phase with parameters k and $m = 10$ to obtain assignment L .
for each pixel label i in L do
 Compute spatial center x_{c_i} , covariance matrix Σ_i , and area κ_i of C_i .
 for each pixel p_j inside of C_i ’s smallest bounding box do
 Generate the variable ξ_{ij} of (P).
Solve (P) for $s_i = x_{c_i}$ to retrieve both primal ξ_{ij}^* , and dual solution $\mu_i^*, \eta_j^*, i \in [k], j \in [N]$.
Set $\mu = (\mu_1^*, \dots, \mu_k^*)$.
return assignment (computed from the ξ_{ij}^*) and diagram parameters $(\Sigma_i^{-1}, x_{c_i}, \mu_i), i \in [k]$.

Algorithm 3. Optimal Power-SLIC.

want to choose μ_i such that $\text{Area}(\|x\|_{\Sigma_i^{-1}}^2 + \mu_i \leq 0) = \kappa_i$ which is equivalent to $\text{Area}(\|x\|_{\Sigma_i^{-1}}^2 \leq -\mu_i) = \kappa_i$.

Since the area of such an ellipsoid is given by $\pi \sqrt{\mu_i^2 \det \Sigma_i}$, we solve $\kappa_i = \pi \sqrt{\mu_i^2 \det \Sigma_i}$ for μ_i and choose the appropriate solution for which $-\mu_i > 0$, hence

$$-\mu_i = \frac{\kappa_i}{\pi \sqrt{\det(\Sigma_i)}}. \quad (3)$$

Our evaluation will show that this choice provides a very good compromise between speed and boundary adherence. (For a use of Eq. (3) in a materials science context, see [36].)

The second observation relates to the fact that the superpixel statistics can be extracted efficiently from the final SLIC assignment iteration without requiring any additional passes over the image data. While this is also true for Optimal Power-SLIC, it becomes particularly relevant with fast implementations of Power-SLIC. In fact, the spatial centers x_{c_1}, \dots, x_{c_k} can be obtained after the final SLIC iteration simply by projecting c_1, \dots, c_k into the spatial image space by dropping their color components. The spatial covariance matrices $\Sigma_1, \dots, \Sigma_k$, can be computed together with the centers within the final iteration of the SLIC assignment, using a single pass algorithm for the variance.

With these parameters, Power-SLIC computes a final assignment that aims at assigning each pixel p_j to its closest spatial center $x_{c_i}, i \in [k]$. Distances are measured in terms of $\|x_{p_j} - x_{c_i}\|_{\Sigma_i^{-1}}^2 + \mu_i$. As in SLIC, we consider only those pixels lying in a $2h \times 2h$ window around the cluster center for the final assignment. In a cleaning step, the still unassigned pixels are assigned to its containing diagram cell. In our experiments, this cleaning step was hardly ever required. Thus, not even a naive implementation would affect

Data: Image, targeted number k of superpixels.
Result: Assignment, GBPD.
Run SLIC’s initialization & assignment phase with parameters k and $m = 10$ to obtain spatial centers x_{c_i} and spatial covariance matrices $\Sigma_i, i \in [k]$.
Compute μ_i using Eq. (3).
Set $L(p_j) = -1$ and $D(p_j) = \infty$ for each pixel p_j .
for each cluster $i \in [k]$ do
 for each pixel p_j in a spatial $2h \times 2h$ window around x_{c_i} do
 if $\|x_{p_j} - x_{c_i}\|_{\Sigma_i^{-1}}^2 + \mu_i < D(p_j)$ then
 Set $D(p_j) = \|x_{p_j} - x_{c_i}\|_{\Sigma_i^{-1}}^2 + \mu_i$.
 Set $L(p_j) = i$.
 for each pixel p_j with $L(p_j) = -1$ do
 Determine cell P_i of the GBPD containing p_j and set $L(p_j) = i$.
return L and diagram parameters $(\Sigma_i^{-1}, x_{c_i}, \mu_i), i \in [k]$.

Algorithm 4. Power-SLIC.

the practical running time. A summary of Power-SLIC is given in Algorithm 4.

Theorem 2 *Power-SLIC runs in $\mathcal{O}(N)$.*

PROOF SLIC’s initialization & assignment phase runs in $\mathcal{O}(N)$, the computation of the diagram parameters is on the fly, and the diagram cell computation for obtaining the superpixels is essentially one additional assignment iteration with a modified distance measure. Thus, we obtain an overall running time of $\mathcal{O}(N)$, which is independent of the number of superpixels k .

6. Evaluation

In this section, we compare Power-SLIC and Optimal Power-SLIC on the Berkeley Segmentation Data Set 500 (BSDS500) [29] with the state-of-the-art superpixel algorithms SLIC [2], SLIC0 [1], NR-SLIC [13], GMMSP [5], Varane [15], ECCPD [27], KIPPI [6], ERS [24], SNIC [3], and SEEDS [38].

Quantitative Evaluation For our quantitative evaluation, we compute boundary recall, undersegmentation error, achievable segmentation accuracy, and compactness for k number of superpixels between 300 and 2,000. Additionally, we report the running times and peak signal-to-noise ratios for image compression for various k . Finally, we measure the noise robustness by considering the trade-off between boundary recall and compactness.

Boundary recall (BR) measures the percentage of detected ground truth boundary pixels. With T_p and F_p de-

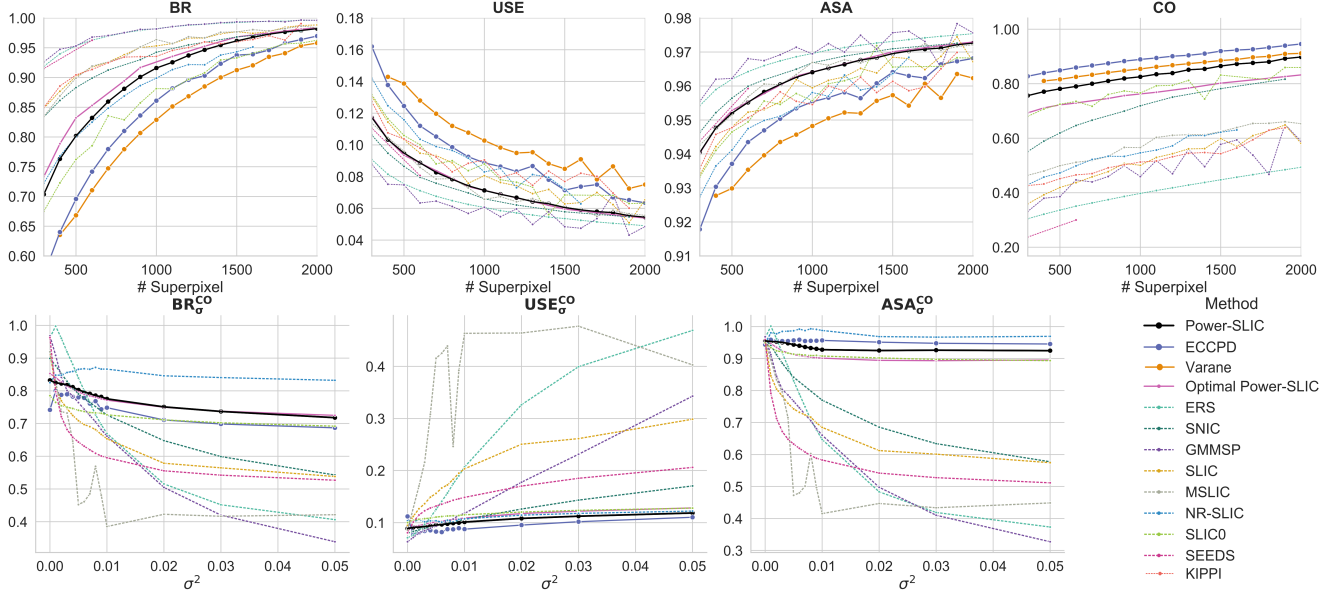


Figure 5. Top: Quantitative comparison of multiple superpixel algorithms. Bottom: Noise robustness of multiple superpixel algorithms and $k = 600$. Here, no results are shown for Varane and KIPPI because the superpixels could not be obtained for noisy images.

noting the number of true positives and false negatives, respectively, BR is defined as $BR = T_p / (T_p + F_n)$. In practice, we follow [2] and classify a ground truth boundary pixel as a true positive if its spatial two-neighborhood contains a superpixel boundary pixel. Accordingly, F_p equals the number of superpixel boundary pixels not in a spatial two-neighborhood of a ground truth boundary pixel.

We also compute the undersegmentation error (USE), which increases when different ground truth regions are grouped into the same superpixel. With \mathcal{G} denoting the set of segments in the ground truth and \mathcal{S} denoting the set of superpixels, USE can be defined as:

$$USE = \frac{1}{\sum_{G \in \mathcal{G}} |G|} \left(\sum_{S \in \mathcal{S}} \sum_{G \in \mathcal{G}} \min(|S \cap G|, |S \setminus G|) \right). \quad (4)$$

The achievable segmentation accuracy (ASA) provides an upper bound on the best obtainable segmentation accuracy of the image when segmenting on the superpixel level. It is defined as

$$ASA = \frac{\sum_{S \in \mathcal{S}} \max_{G \in \mathcal{G}} |S \cap G|}{\sum_{G \in \mathcal{G}} |G|}. \quad (5)$$

To evaluate compactness, we compute the compactness of the superpixels as introduced in [34]. Let b_i and κ_i denote the i th superpixel's total number of boundary pixels and area. With Q_i the iso-perimetric quotient, compactness (CO) is defined as:

$$Q_i = \frac{4\pi\kappa_i}{b_i^2}, \quad CO = \sum_{i=1}^k Q_i \frac{\kappa_i}{N}. \quad (6)$$

Compactness essentially measures the similarity of the superpixels to a disc.

Figure 5 provides a comparison among the superpixels algorithms. First, note that the algorithms Varane, ECCPD, and (Optimal) Power-SLIC are the only algorithms that compute a low-dimensional diagram representation of the superpixels. As these superpixels are diagram cells, they result in high compactness values.

While Power-SLIC generates slightly less compact superpixels than Varane and ECCPD, it outperforms the diagram approaches in BR, USE, and ASA for any number k of superpixels. Remarkably, Power-SLIC's performance in these categories falls into the range achieved by pixel methods.

Pixel methods are often highly sensitive to changing image conditions and can fail when small amounts of noise are present in the image. For example, looking at GMMSP in Fig. 6 its superpixel segmentation degenerates quite considerably if noise is added: The algorithm identifies too many image boundaries, and almost all pixels are identified as boundaries. While this results in a high boundary recall by definition, the segmentation deteriorates and the compactness value decreases significantly. It is therefore reasonable to penalize the measures BR, ASA, USE for a decreasing compactness value; see [27], which also relates the measures to the compactness value. Let CO_{σ} denote the compactness value for the noise level σ^2 . Similarly, we denote by BR_{σ} , ASA_{σ} , USE_{σ} the measures at noise level σ^2 . We

		$k=500$	$k=1,000$	$k=1,500$	$k=2,000$
Time (in s)	Varane	2.549	10.191	18.620	47.022
	ECCPD	28.703	96.408	149.929	171.321
	Power-SLIC	0.070	0.074	0.078	0.080
PSNR	Varane	29.667	29.998	30.271	30.318
	ECCPD	29.716	30.101	30.369	30.259
	Power-SLIC	30.201	30.578	30.840	31.027

Table 1. Top: Running times on a laptop with an Intel Core i7 5600U processor. Bottom: Peak signal-to-noise ratios.

define

$$BR_\sigma^{CO} = BR_\sigma \cdot \frac{CO_\sigma}{CO_0}, \quad ASA_\sigma^{CO} = ASA_\sigma \cdot \frac{CO_\sigma}{CO_0},$$

$$USE_\sigma^{CO} = USE_\sigma \cdot \frac{CO_0}{CO_\sigma}.$$

In other words, we consider the compactness relatively to the compactness for noise-free images so that the measures do not depend on the compactness of the superpixel segmentation for noise-free images. For a perfectly noise-robust superpixel algorithm, we expect the measures to be constant and therefore independent of σ . Figure 5 summarizes the results for $k = 600$ (a similar behavior is observed for other typical values of k). We observe that NR-SLIC, an algorithm specifically designed for noisy images, performs best overall. On the other hand, those algorithms with very high boundary recall on clean images tend to deteriorate quickly, even for small amounts of noise ($\sigma^2 < 0.01$), mainly because they detect too many ‘‘image boundaries’’ in the noisy cases (see also Fig. 6). Power-SLIC and ECCPD are relatively robust to noise, and their performance decreases only slightly with increasing noise.

We now focus on two aspects of the diagram approaches. First, we measure computational speed, a bottleneck of diagram methods so far. Second, we assess the compression quality achieved by the highly sparsely-encoded superpixel segmentation provided by diagrams.

Timings are shown in Tab. 1. Power-SLIC is several orders of magnitude faster than the other diagram approaches and its running time increases only slightly with k .

As mentioned above, diagram approaches are particularly suited to provide sparse image encodings on which one can base subsequent higher-level computer vision tasks or employ them for image compression [27]. Using Power-SLIC, for instance, one can represent and store an image by specifying $9k$ (floating point) parameters: for each superpixel, two for its cell site, three for covariance matrix, one for the size parameter, and three for the average color.

Following papers such as [27], we evaluate the quality of the generated sparse image representation by reporting the peak signal-to-noise ratio (PSNR) between the original and compressed image. With x_{p_j} and \hat{x}_{p_j} denoting the color

	Diagram	Fast	Compact	Noise-Robust
Power-SLIC	✓	✓	✓	✓
Varane	✓	-	✓	-
ECCPD	✓	-	✓	✓
ERS	-	✓	-	-
SNIC	-	✓	✓	-
GMMSP	-	✓	-	-
SLIC	-	✓	-	-
MSLIC	-	✓	-	-
NR-SLIC	-	✓	-	✓
SLIC0	-	✓	✓	✓
KIPPI	-	✓	-	-
SEEDS	-	✓	-	-

Table 2. Qualitative comparison of multiple superpixel algorithms.

value of the j -th pixel in the original and compressed image, respectively. the PSNR is defined as

$$MSE = \frac{1}{3N} \sum_{j=1}^N \|x_{p_j} - \hat{x}_{p_j}\|_2^2, \quad (7)$$

$$PSNR = 10 \cdot \log_{10} \left(\frac{255^2}{MSE} \right). \quad (8)$$

Larger PSNR values indicate a better quality of the compressed image. The resulting PSNR values for the BSDS500 dataset are shown in Tab. 1. In all cases, Power-SLIC gives the highest PSNR values despite having the smallest running times. It seems that the anisotropic diagram structure, involving quadratic boundaries, allows Power-SLIC to improve on Varane and ECCPD, both of which use less flexible diagram classes.

Qualitative Evaluation Table 2 provides a qualitative comparison of multiple superpixel algorithms. (Algorithms are classified as ‘diagram-based,’ ‘fast,’ ‘noise-robust,’ and ‘compact’ if their superpixels are described by diagram cells, their average running times for $k = 500$ are below 1s, all their plots in Fig. 5 are close to horizontal lines, and their plots are in the top of the two groups for compactness in Fig. 5.) Figure 6 gives a qualitative comparison of ten superpixel algorithms for varying levels of noise.

A comparison of the post-processing steps of Power-SLIC and SLIC is given in Fig. 7. Although Power-SLIC uses SLIC’s clustering approach, it is notable that the superpixels are fundamentally different due to the post-processing step. This difference can be seen by comparing the results with the second column of Fig. 7, which depicts the clustering result of SLIC without any post-processing. Only the local post-processing by SLIC shown in the third column creates a reasonable segmentation, which deteriorates for more extensive noise levels. In contrast, Power-SLIC optimizes more globally and returns a diagram representation. At the same time, this approach acts as a regularizer for high noise levels.

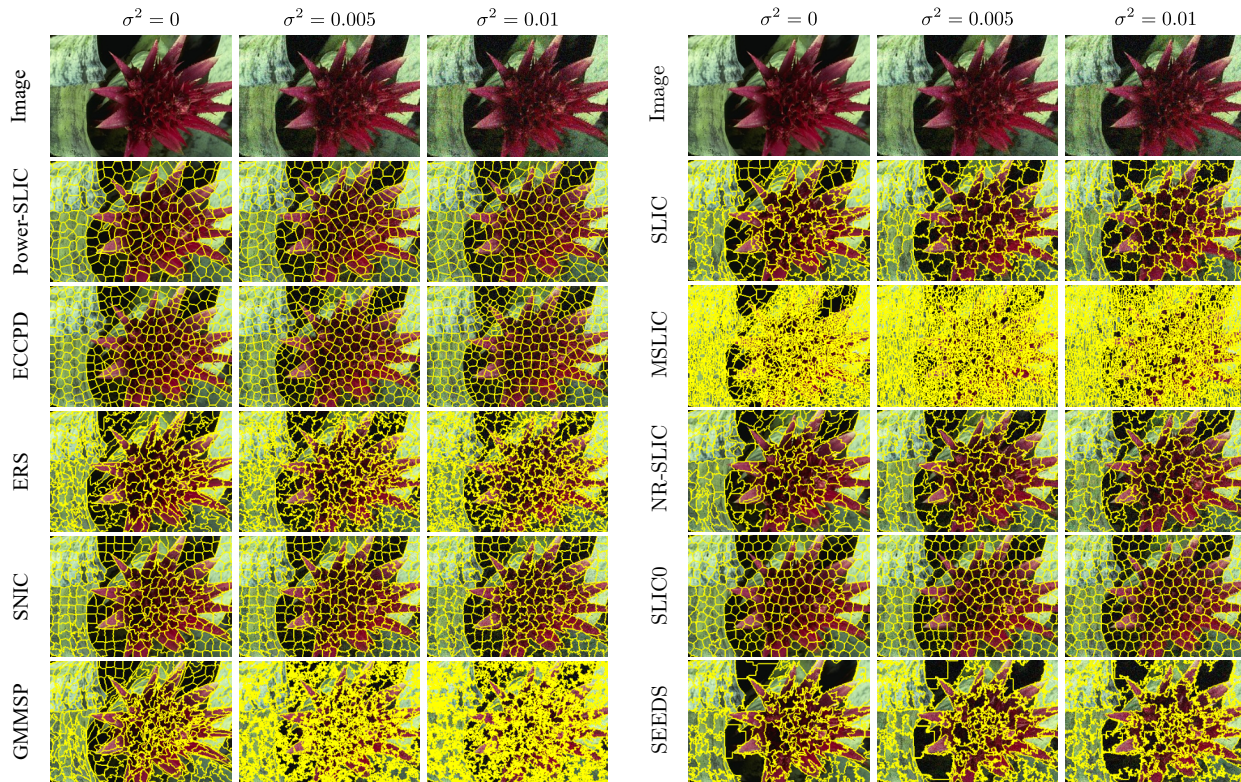


Figure 6. Visual comparison of five superpixel algorithms for various levels of noise ($k = 700$).

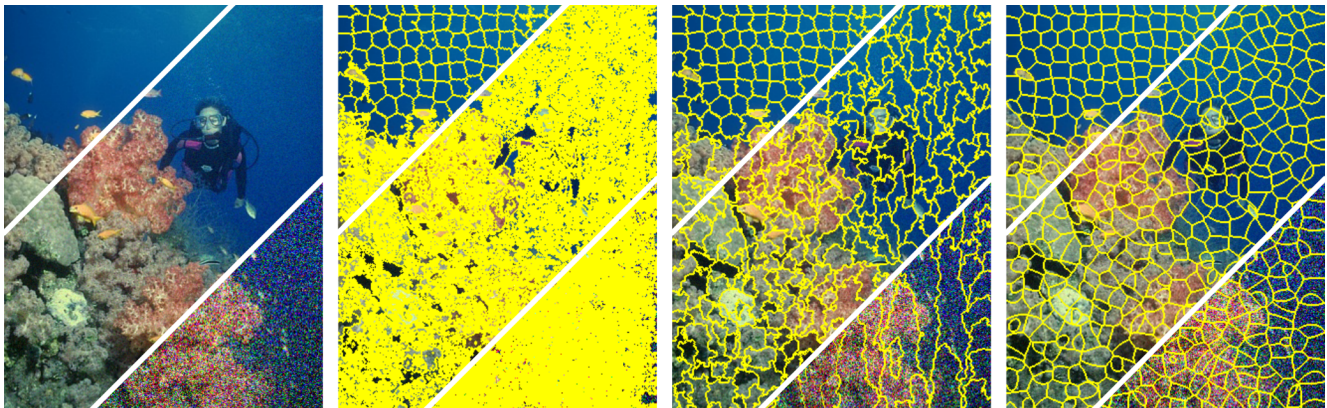


Figure 7. Algorithms applied to an image with three levels of noise $\sigma^2 \in \{0, 0.001, 0.1\}$ and $k = 700$. Left to right: original image, SLIC before post-processing, SLIC, and Power-SLIC.

7. Conclusion

We presented a new superpixel algorithm, called Power-SLIC, whose superpixels are described by cells of diagrams. Using GBPDs, the quadratic boundaries appear to provide enough flexibility to capture complex image boundaries, while providing sufficient regularization to obtain very compact superpixels. This results in a high level of robustness under varying levels of additive white Gaussian

noise. Additionally, Power-SLIC matches the running times of SLIC in theory and practice. Power-SLIC's added benefit of being resolution-independent can be used to speed up superpixel generation for larger images, as a full segmentation can be computed on a low-resolution version of the image.

References

- [1] R. Achanta, A. Shaji, K. Smith, A. Lucchi, P. Fua, and S. Süsstrunk. <https://www.epfl.ch/labs/ivrl/research/slic-superpixels/>. 2, 5
- [2] R. Achanta, A. Shaji, K. Smith, A. Lucchi, P. Fua, and S. Süsstrunk. SLIC superpixels compared to state-of-the-art superpixel methods. *IEEE Trans. Pattern Anal. Mach. Intell.*, 34(11):2274–2282, 2012. 1, 2, 3, 5, 6
- [3] R. Achanta and S. Süsstrunk. Superpixels and polygons using simple non-iterative clustering. In *Proc. Int. Conf. Computer Vision and Pattern Recognition (CVPR)*, pages 4895–4904. IEEE, 2017. 2, 3, 5
- [4] A. Alpers, A. Brieden, P. Gritzmann, A. Lyckegaard, and H. F. Poulsen. Generalized balanced power diagrams for 3D representations of polycrystals. *Philos. Mag.*, 95(9):1016–1028, 2015. 2, 3, 4
- [5] Z. Ban, J. Liu, and L. Cao. Superpixel segmentation using Gaussian mixture model. *IEEE Trans. Image Process.*, 27(8):4105–4117, 2018. 1, 2, 5
- [6] J.-P. Bauchet and F. Lafarge. KIPPI: KInetic Polygonal Partitioning of Images. In *Proc. Int. Conf. Computer Vision and Pattern Recognition (CVPR)*, pages 3146–3154. IEEE, 2018. 2, 3, 5
- [7] B. Brekhna, A. Mahmood, Y. Zhou, and C. Zhang. Robustness analysis of superpixel algorithms to image blur, additive Gaussian noise, and impulse noise. *J. Electron. Imaging*, 26(6):061604, 2017. 2
- [8] A. Brieden and P. Gritzmann. On clustering bodies: geometry and polyhedral approximation. *Discrete Comput. Geom.*, 44(1):508–534, 2010. 2, 4
- [9] A. Brieden and P. Gritzmann. On optimal weighted balanced clusterings: gravity bodies and power diagrams. *SIAM J. Discrete Math.*, 26(2):415–434, 2012. 4
- [10] A. Brieden, P. Gritzmann, and F. Klemm. Constrained clustering via diagrams: A unified theory and its applications to electoral district design. *Eur. J. Oper. Res.*, 263(1):18–34, 2017. 4
- [11] Y. Cai and X. Guo. Anisotropic superpixel generation based on Mahalanobis distance. *Comput. Graph. Forum*, 35(7):199–207, 2016. 2
- [12] Z. Chen, Y. Xiao, and J. Cao. Approximation by piecewise polynomials on Voronoi tessellation. *Graph. Models*, 76(5):522–531, 2014. 2
- [13] L. Dong and J. Zhou. Noise-robust SLIC superpixel for natural images. In *Proc. Int. Conf. Cloud Computing and Big Data (CCBD)*, pages 335–340. IEEE, 2016. 2, 5
- [14] L. Duan and F. Lafarge. Varane implementation. <https://www-sop.inria.fr/members/Florent.Lafarge/codes.html>. 2
- [15] L. Duan and F. Lafarge. Image partitioning into convex polygons. In *Proc. Int. Conf. Computer Vision and Pattern Recognition (CVPR)*, pages 3119–3127. IEEE, 2015. 2, 5
- [16] J.-D. Favreau, F. Lafarge, A. Bousseau, and A. Auvolat. Extracting geometric structures in images with delaunay point processes. *IEEE Trans. Pattern Anal. Mach. Intell.*, 42(4):837–850, 2020. 3
- [17] J. Forsythe, V. Kurlin, and A. W. Fitzgibbon. Resolution-independent superpixels based on convex constrained meshes without small angles. In *Proc. Int. Symp. Vis. Comp. (ISVC)*, pages 223–233. Springer, 2016. 2, 3
- [18] O. Freifeld, Y. Li, and J. W. Fisher. A fast method for inferring high-quality simply-connected superpixels. In *Proc. Int. Conf. Image Processing (ICIP)*, pages 2184–2188. IEEE, 2015. 2
- [19] B. Fulkerson, A. Vedaldi, and S. Soatto. Class segmentation and object localization with superpixel neighborhoods. In *Proc. Int. Conf. Computer Vision (ICCV)*, pages 670–677. IEEE, 2009. 1
- [20] S. Gould, J. Rodgers, D. Cohen, G. Elidan, and D. Koller. Multi-class segmentation with relative location prior. *Int. J. Comput. Vis.*, 80(3):300–316, 2008. 1
- [21] LLC Gurobi Optimization. Gurobi optimizer reference manual, 2020. 4
- [22] V. Kurlin and G. Muszynski. Persistence-based resolution-independent meshes of superpixels. *Pattern Recognit. Lett.*, 131(1):300–306, 2020. 2, 3
- [23] A. Levinshtein, A. Stere, K. N. Kutulakos, D. J. Fleet, S. J. Dickinson, and K. Siddiqi. TurboPixels: Fast superpixels using geometric flows. *IEEE Trans. Pattern Anal. Mach. Intell.*, 31(12):2290–2297, 2009. 2
- [24] M.-Y. Liu, O. Tuzel, S. Ramalingam, and R. Chellappa. Entropy rate superpixel segmentation. In *Proc. Int. Conf. Computer Vision and Pattern Recognition (CVPR)*, pages 2097–2104. IEEE, 2011. 2, 5
- [25] Y.-J. Liu, C.-C. Yu, M.-J. Yu, and Y. He. Manifold SLIC: A fast method to compute content-sensitive superpixels segmentation. In *Proc. Int. Conf. Computer Vision and Pattern Recognition (CVPR)*, pages 651–659. IEEE, 2016. 2
- [26] Y.-J. Liu, M. Yu, B.-J. Li, and Y. He. Intrinsic Manifold SLIC: A simple and efficient method for computing content-sensitive superpixels. *IEEE Trans. Pattern Anal. Mach. Intell.*, 40(3):653–666, 2017. 2
- [27] D. Ma, Y. Zhou, S. Xin, and W. Wang. Convex and compact superpixels by edge-constrained centroidal power diagram. *IEEE Trans. Image Process.*, 30:1825–1839, 2021. 2, 5, 6, 7
- [28] S. R. S. P. Malladi, S. Ram, and J. J. Rodriguez. Image denoising using superpixel-based PCA. *IEEE Trans. Multimed.*, 23:2297–2309, 2020. 1
- [29] D. Martin, C. Fowlkes, D. Tal, and J. Malik. A database of human segmented natural images and its application to evaluating segmentation algorithms and measuring ecological statistics. In *Proc. Int. Conf. Computer Vision (ICCV)*, pages 416–423. IEEE, 2001. 5
- [30] W. Menze and A. Geiger. Object scene flow for autonomous vehicles. In *Proc. Int. Conf. Computer Vision and Pattern Recognition (CVPR)*, pages 3061–3070. IEEE, 2015. 1
- [31] G. Mori. Guiding model search using segmentation. In *Proc. Int. Conf. Computer Vision (ICCV)*, pages 1417–1423. IEEE, 2005. 1
- [32] X. Ren and J. Malik. Learning a classification model for segmentation. In *Proc. Int. Conf. Computer Vision (ICCV)*, pages 10–17. IEEE, 2003. 1, 2

- [33] J. Roels, J. De Vylder, J. Aelterman, S. Lippens, Y. Saeys, and W. Philips. Superpixel quality in microscopy images: The impact of noise & denoising. In *Proc. XIV Mediterranean Conf. Medical and Biological Engineering and Computing (MEDICON)*. Springer, 2016. [2](#)
- [34] A. Schick, M. Fischer, and R. Stiefelhagen. Measuring and evaluating the compactness of superpixels. In *Proc. Int. Conf. Pattern Recognition (ICPR)*, pages 930–934. IEEE, 2012. [6](#)
- [35] D. Stutz, A. Hermans, and B. Leibe. Superpixels: An evaluation of the state-of-the-art. *Comput. Vis. Image Underst.*, 166:1–27, 2018. [1](#), [2](#)
- [36] K. Teferra, , and D. J. Rowenhorst. Direct parameter estimation for generalised balanced power diagrams. *Philos. Mag. Lett.*, 98(2):79–87, 2018. [2](#), [5](#)
- [37] R. Uziel, M. Ronen, and O. Freifeld. Bayesian adaptive superpixel segmentation. In *Proc. Int. Conf. Computer Vision (ICCV)*, pages 8470–8479. IEEE, 2019. [2](#)
- [38] M. van den Bergh, X. Boix, G. Roig, B. de Capitani, and L. van Gool. SEEDS: Superpixels extracted via energy-driven sampling. In *Proc. Europ. Conf. Computer Vision (ECCV)*, pages 13–26. Springer, 2012. [2](#), [5](#)
- [39] J. Wang and X. Wang. VCells: Simple and efficient superpixels using edge-weighted centroidal Voronoi tessellations. *IEEE Trans. Pattern Anal. Mach. Intell.*, 34(6):1241–1247, 2012. [2](#)
- [40] M. Wang, X. Liu, Y. Gao, X. Ma, and N. Q. Soomro. Superpixel segmentation: A benchmark. *Signal Process. Image Commun.*, 56:28–39, 2017. [2](#)
- [41] S. Wang, H. Lu, F. Yang, and M.-H. Yang. Superpixel tracking. In *Proc. Int. Conf. Computer Vision (ICCV)*, pages 1323–1330. IEEE, 2011. [1](#)
- [42] C. L. Zitnick and S. B. Kang. Stereo for image-based rendering using image over-segmentation. *Int. J. Comput. Vis.*, 75(1):49–65, 2007. [1](#)